JGR Atmospheres

RESEARCH ARTICLE
10.1029/2020JD032784

Investigation of Isoprene Dynamics During the Day-to-Night Transition Period

Dandan Wei[1], Hariprasad D. Alwe[2], Dylan B. Millet[2], Sarah C. Kavassalis[3], Michelle Lew[4], Brandon Bottorff[4], Philip S. Stevens[4,5], and Allison L. Steiner[1]

[1]Department of Climate and Space Sciences and Engineering, University of Michigan, Ann Arbor, MI, USA, [2]Department of Soil, Water and Climate, University of Minnesota, Twin Cities, St. Paul, MN, USA, [3]Department of Chemistry, University of Toronto, Toronto, Ontario, Canada, [4]Department of Chemistry, Indiana University, Bloomington, IN, USA, [5]School of Public and Environmental Affairs, Indiana University, Bloomington, IN, USA

Key Points:
- Low turbulent mixing during clear and calm nights leads to accumulation of isoprene within the canopy
- Turbulent mixing accounts for 80% of the observed nighttime isoprene loss rates
- Isoprene flux measurements did not capture the majority of the removal of the accumulated isoprene

Correspondence to:
D. Wei,
dandanwe@umich.edu

Citation:
Wei, D., Alwe, H. D., Millet, D. B., Kavassalis, S. C., Lew, M., Bottorff, B., et al. (2020). Investigation of isoprene dynamics during the day-to-night transition period. *Journal of Geophysical Research: Atmospheres*, *125*, e2020JD032784. https://doi.org/10.1029/2020JD032784

Received 20 MAR 2020
Accepted 2 OCT 2020
Accepted article online 14 OCT 2020

Abstract At the University of Michigan Biological Station during the 2016 AMOS field campaign, isoprene concentrations typically peak in the early afternoon (around 15:00 local time, LT) under well-mixed conditions. However, an end-of-day peak (around 21:00 LT) occurs on 23% of the campaign days, followed by a rapid removal (from 21:00–22:00 LT) at rate of 0.57 hr^{-1} during the day-to-night transition period. During the end-of-day peak, in-canopy isoprene concentrations increase by 77% (from 3.5 to 6.2 ppbv) on average. Stratification and weak winds (<3.4 m s^{-1} at 46 m) significantly suppress turbulent exchanges between in- and above-canopy, leading to accumulation of isoprene emitted at dusk. A critical standard deviation of the vertical velocity (σ_w) of 0.14, 0.2, and 0.29 m s^{-1} is identified to detect the end-of-day peak for the height of 13, 21, and 34 m, respectively. In 85% of the end-of-day cases, the wind speed increases above 2.5 m s^{-1} after the peak along with a shift in wind direction, and turbulence is reestablished. Therefore, the wind speed of 2.5 m s^{-1} is considered as the threshold point where turbulence switches from being independent of wind speed to dependent on wind speed. The reinstated turbulence accounts for 80% of the subsequent isoprene removal with the remaining 20% explained by chemical reactions with hydroxyl radicals, ozone, and nitrate radicals. Observed isoprene fluxes do not support the argument that the end-of-day peak is reduced by vertical turbulent mixing, and we hypothesize that horizontal advection may play a role.

1. Introduction

Isoprene accounts for almost half of the nonmethane biogenic volatile organic compound (BVOCs) fluxes emitted to the atmosphere globally (Guenther et al., 2012). Isoprene substantially influences hydroxyl radical (OH) concentration in the atmosphere and thus atmospheric oxidative capacity and tropospheric chemistry (Fuchs et al., 2013; Taraborrelli et al., 2012). In addition, because of the large flux of isoprene into the atmosphere (Guenther et al., 2012), oxidation of isoprene is a significant source of secondary organic aerosols (SOA) with implication for air quality and climate (Claeys, 2004; Robinson et al., 2011). While daytime isoprene has been studied thoroughly, its day-to-night transition has received little attention. The near-zero emissions during the transition period allow us to better quantify processes responsible for isoprene loss, which is critical for accurate estimation of nighttime chemistry and SOA formation (especially nitrate SOA Ng et al., 2008).

Daytime isoprene concentrations shows pronounced diurnal cycles with a peak in the early afternoon (around 15:00 local time) in response to sources (e.g., emission) and sinks (e.g., turbulent mixing and chemical reactions). Isoprene emission from plants is linked to photosynthesis and thus highly temperature and light dependent. As a result, isoprene emission peaks around noon and shuts down after sunset (Guenther et al., 1993). After being emitted into the atmosphere, isoprene is redistributed by turbulent mixing and at the same time chemically consumed by OH, ozone (O_3), and nitrate radicals (NO_3). Since the O_3 reaction is slow (τ = 30 hr at [O_3] = 30 ppbv) and NO_3 mainly exists at night, OH is considered to be the major chemical sink of isoprene during the daytime (Lelieveld et al., 2008; Levy, 1971). OH is photolytically produced and its concentrations drop significantly at sunset due to reduced radiation. Given that the loss of isoprene to OH diminishes toward the end of the day (τ = 11.5 hr at [OH] = 2.42×10^5 molecules cm^{-3}, 2016 AMOS

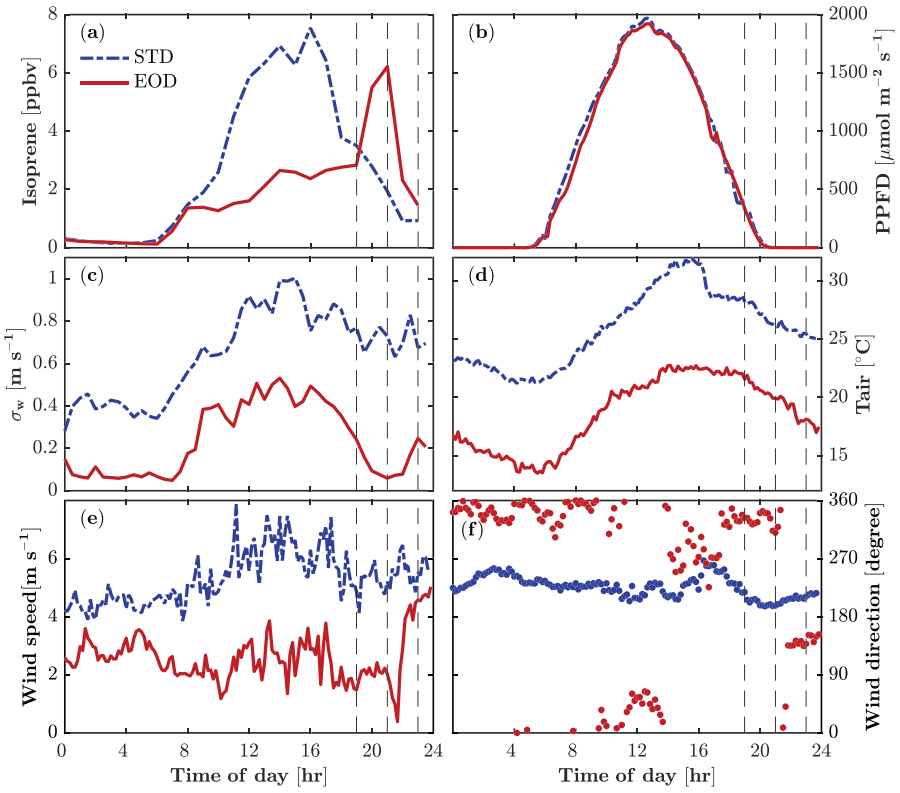

Figure 1. Examples of the end-of-day peak case (EOD; 19 July 2016) and the standard case (STD; 13 July 2016). (a) Diurnal variations of hourly isoprene mixing ratios (ppbv) at 21 m. (b) Diurnal variations of 10 min photosynthetic phototon flux density (PPFD) at 46 m. (c) Diurnal variations in half hourly standard deviation of vertical velocity (σ_w) at 21 m. (d) Diurnal variations in 10 min air temperature at 46 m. (e) Diurnal variations in hourly isoprene flux at 34 m. (f) Diurnal variations in 10 min wind speed (line) and wind direction (dot) at 46 m.

campaign average for 19:00 local time), turbulent mixing of isoprene emitted close to dusk plays an important role in shaping the nocturnal isoprene mixing ratios.

An end-of-day (EOD) peak was frequently observed around 21:00 local time (LT) during the AMOS (Atmospheric Measurements of Oxidants in Summer) field campaign, followed by a precipitous decay in isoprene from 21:00–22:00 LT (Figure 1a). In this study, we aim to (i) characterize the EOD peak and understand its origin and (ii) constrain the possible mechanisms responsible for the rapid decline in isoprene. As for the EOD peak, previous field studies have reported elevated surface isoprene concentrations during the early evening in various locations (Goldan et al., 1995; Martin et al., 1991; Montzka et al., 1993; Starn et al., 1998). Martin et al. (1991) observed that peak isoprene concentrations at Scotia, Pennsylvania, occurred at 20:00 local time, at levels 2–3 times those observed at noon. Starn et al. (1998) interpreted elevated isoprene concentrations as a result of advective transport to the measurement site. But little quantitative explanations for the EOD isoprene peak are provided by previous studies. As for the subsequent decay, rapid isoprene removal during the day-to-night transition period has been frequently observed in forested environments. Due to the lack of constraints from reliable measurements, the cause of this rapid decrease in isoprene has been attributed to chemical loss (Faloona et al., 2001) or dynamics (Apel, 2002; Sillman et al., 2002). Hurst et al. (2001) estimated that either OH or vertical mixing could be the reason for this phenomenon, but no direct measurements were available to differentiate the two processes. Faloona et al. (2001) observed abnormally high OH concentrations at night, suggesting OH was responsible for the rapid decay in isoprene, but interferences for this OH instrument were later reported (Feiner et al., 2016). Apel (2002) and Sillman et al. (2002) postulated vertical dilution or horizontal advection could explain the rapid removal, but no turbulence data existed to support the speculation.

During the day-to-night transition period, organization of canopy flows in forested sites falls into two major categories: (i) well-mixed conditions where the turbulence is continuous down to the ground and (ii) more

stable conditions as the canopy begins to cool, characterized by a temperature inversion and turbulence suppressed on all scales (Mahrt, 1999). On clear and calm nights, thermal stratification and weak mechanical production of turbulence favor the generation of such stable conditions (Van de Wiel, Moene, & Jonker, 2012; Van de Wiel, Moene, Jonker, Baas, et al., 2012) under which the above- and in-canopy air layer exchanges are significantly weakened (commonly known as decoupling). Early-evening decoupling has been observed frequently (at least 31% of the summer nighttime periods Alekseychik et al., 2013) at various forested sites (Alekseychik et al., 2013; Burns et al., 2010; van Gorsel et al., 2011; Oliveira et al., 2012). Smaller biogenic fluxes and larger gradients in temperature and scalar concentration between above- and in-canopy layers coincide with decoupling conditions due to reduced mixing (Alekseychik et al., 2013; Oliveira et al., 2012).

However, overnight turbulence generation can lead to a breakdown of the decoupling state, allowing for recoupling and mixing between the canopy interior and the air above it (Alekseychik et al., 2013; Oliveira et al., 2012). During the aforementioned decoupling period, nonstationary motions (such as density currents, drainage flow, and canopy waves) dominate (Mahrt et al., 2012; Sun et al., 2012) and turbulence is weak, intermittent and independent of the mean wind speed (Liang et al., 2014). However, evidence suggests that there is a "threshold" point at which stable-condition turbulence switches from being independent of wind speed to being dependent on wind speed (Liang et al., 2014; Mahrt et al., 2012; Sun et al., 2012). The resultant wind-induced turbulence significantly affects the nighttime vertical profile of scalars as well as scalar flux determination (Oliveira et al., 2012). Therefore, wind speed and the resultant turbulence are then expected to influence the vertical gradient of isoprene during the transition period.

The 2016 AMOS campaign at UMBS (University of Michigan Biological Station) provide detailed measurements of isoprene and its oxidants (i.e., OH, NO_3, O_3) as well as meteorological and turbulence data, which allow us to fill in the gaps in our knowledge of the chemical and physical processes governing isoprene dynamics during the day-to-night transition period. In the present study, we compare two distinct isoprene patterns during the transition period to show the characteristics and origin of the EOD isoprene peak. We also discuss and constrain possible mechanisms for the subsequent isoprene removal to illuminate the relative importance of turbulence and chemistry on nocturnal distribution of reactive gases in forested environment.

2. Methods

2.1. Study Site

The 2016 AMOS field campaign was conducted in the UMBS site located near the northern end of the lower peninsula of Michigan, United States, during the month of July. The UMBS site is a mixed deciduous/coniferous forest and isoprene-dominated (Millet et al., 2018). It is surrounded by the Great Lakes, with Lake Superior 21 km to the north, Lake Michigan 35 km to the west, and Lake Huron 42 km to the east. In addition, there are smaller lakes scattered within 3 km of the site. For example, Douglas Lake is less than 200 m to the north of the UMBS site, and Burt Lake is about 2.5 km south of the site. There was little indication of local anthropogenic pollution in the surrounding area during the field campaign (NO < 0.1 ppbv), although the region is frequently impacted by the transport of NO_X from urban areas to the south and west (e.g., Milwaukee, Chicago, Detroit Cooper et al., 2001; VanReken et al., 2015) as well as long-range transport of smoke pollution from Canada (Cooper et al., 2001; Gunsch et al., 2018). The 31 m PROPHET (Program for Research on Oxidants: PHotochemistry, Emissions, and Transport) tower extends to 34 m with a triangle tower on top. The canopy height surrounding the tower is about 22.5 m.

2.2. Measurements

Turbulence data (10 Hz) were collected at five heights on the PROPHET tower: 34 m (CSAT 3B, Campbell Scientific Inc.), 29 m (81000, RM Young), 21 m (CSAT 3, Campbell Scientific Inc.), 13 m (CSAT 3, Campbell Scientific Inc.), and 5 m (CSAT 3, Campbell Scientific Inc.). High-frequency data outside of 3.5 standard deviations were removed and data then were separated into 30 min windows to apply a tilt correction (Foken, 2009). The 30 min periods that experienced rain (as measured by the rain gauge at the UMBS AmeriFlux tower), weak winds (<0.5 m s^{-1} at the top sonic anemometer), and wind directed through the tower were excluded due to potential interference. Other meteorologial measurements (at 46 m) used here include photosynthetic photon flux densities (PPFD) measured at the US-UMB Ameriflux tower (about 130 m from the PROPHET tower) using a BF5 Sunshine Sensor (Delta-T Devices Ltd.), air temperature

measured with a Vaisala HMP-60 in a six-plate radiation shield at the top of the PROPHET tower, and wind speed and direction.

Measurements of isoprene and other volatile organic compounds (VOCs) were performed by PTR-QiTOF (Ionicon Analytik, GmbH) from six sampling heights on the PROPHET tower: 34, 21, 17, 13, 9, and 5 m (Alwe et al., 2019; Millet et al., 2018). The measurement sequence cycled hourly between these inlets using a custom-built automated sampling manifold, with 30 min per hour spent sampling from the 34 m inlet and 5 min per hour from the remaining five inlets. The remaining 5 min of each hour was used to perform a measurement blank. It is therefore an approximation to treat the vertical gradient of isoprene as a complete gradient at a single point in time, because it reflects sequential measurements. Thirty days of isoprene data were obtained. We excluded the cloudy and rainy days, and identified seven cases with EOD peaks and seven cases with early-afternoon peaks (hereafter referred to as standard cases). Turbulence measurements performed at the 34 m isoprene sampling inlet were used to compute hourly isoprene fluxes. Details of the isoprene measurements and calibration can be found in Millet et al. (2018).

Other chemical measurements at the PROPHET tower implemented in this study include OH (hydroxyl radical) and O_3 (ozone) concentrations. O_3 were measured at 6 m using a Model 205 (2B Technologies, Inc.) dual-beam UV absorption instrument. OH radicals were measured at the top of the PROPHET tower at a height of 32 m using the Indiana University Laser-Induced Fluorescence-Fluorescence Assay by Gas Expansion (LIF-FAGE) instrument (Dusanter et al., 2009). To quantify potential interferences during ambient measurements of OH, perfluoropropylene (C_3F_6) was added above the sampling nozzle using an automated injector to chemically remove ambient OH radicals (Griffith et al., 2016; Rickly & Stevens, 2018). Any signal measured during C_3F_6 addition thus provided a quantification of instrumental interferences. During PROPHET-AMOS, no unknown interferences were detected during the campaign using this method.

2.3. Data Analysis

2.3.1. Virtual Potential Temperature

Virtual potential temperature (θ_v) was calculated using the equation below:

$$\theta_v = T_v\left(\frac{p_0}{p}\right)^{\kappa} \tag{1}$$

where T_v is the virtual temperature, p_0 is the standard pressure at sea level (1,013.25 hPa), p is the air pressure at the height of T_v, and κ is the Poisson constant (0.2854). In the present study, we used the sonic temperature (T_s) from the sonic anemometers as the virtual temperature (T_v) because they are almost equal (Rebmann et al., 2011). Two levels of pressure data (6 and 34 m) are available. The 6 m pressure data were used for the calculations of θ_v within the canopy (at 5, 13, and 21 m), and the 34 m pressure data for the above-canopy (at 29 and 36 m) calculations.

2.3.2. Turbulent Mixing Time Scale

A mass balance approach was employed to calculate the turbulent mixing timescale for isoprene. Assuming horizontal homogeneity, the mass balance for the isoprene mixing ratio can be expressed as (Freire et al., 2017)

$$\frac{\partial[\mathrm{ISOP}]}{\partial t} = -\frac{\partial w'[\mathrm{ISOP}]'}{\partial z} + S(z) \tag{2}$$

where $S(z)$ is the source/sink term. An eddy diffusivity (K) model ($w'[\mathrm{ISOP}]' = -K\frac{\partial[\mathrm{ISOP}]}{\partial z}$) is employed in Equation 2, and the term of vertical gradients in eddy diffusivity ($\frac{\partial K}{\partial z}$) is neglected for simplicity and analytical tractability. The assumption of $\frac{\partial K}{\partial z} = 0$ is imposed to the domain $h < z < z_0$ (h is the canopy height, and z_0 is the top of the stable boundary layer). Then Equation 2 reduces to

$$\frac{\partial[\mathrm{ISOP}]}{\partial t} = -K\frac{\partial^2[\mathrm{ISOP}]}{\partial z^2} + S(z) \tag{3}$$

The homogeneous solution ($S = 0$) to Equation 3 represents the time evolution of the isoprene mixing ratio due to turbulent mixing in the domain $h < z < z_0$. A solution subject to the initial condition $[\mathrm{ISOP}](z, t = 0) = 0$, the lower boundary condition $[\mathrm{ISOP}](z = h, t) = [\mathrm{ISOP}]_h$, and the upper boundary condition of a

zero isoprene flux at $z = z_0$ is sought. In this case, the transient solution for the isoprene mixing ratio above the canopy can be expressed as Liu (2008)

$$\frac{[\mathrm{ISOP}](z,t)}{[\mathrm{ISOP}]_h} = 1 - \sum_{n=0}^{\infty} \frac{4}{(2n+1)\pi} \exp\left\{ -\left(\frac{(2n+1)\pi}{2}\right)^2 \frac{K(z)t}{(z_0-h)^2} \right\} \sin\left[\frac{(2n+1)\pi}{2}\frac{z-h}{z_0-h}\right] \quad (4)$$

A height-dependent turbulent mixing time scale can be obtained from Equation 4 by finding the time required for the isoprene mixing ratio to reach a certain fraction of the imposed value at the top of the canopy. In the present study, the turbulent mixing time scale is defined as the time required for $\frac{[\mathrm{ISOP}](z)}{[\mathrm{ISOP}]_h} = 0.95$. This value of 0.95 was obtained using the vertical gradients of isoprene observed in the standard (STD) case (see section 2.2) to represent well-mixed conditions. The inverse of the turbulent mixing timescale is then used as the isoprene loss rate associated with turbulent mixing.

3. Results

3.1. EOD Peak in Isoprene

3.1.1. Case Studies

Here we define two classes of diurnal isoprene profiles: (i) the EOD (EOD) case where isoprene increased at dusk (one of the seven identified cases displayed in Figure 1a) and (ii) a standard (STD) diurnal cycle (one of the seven identified cases displayed in Figure 1a). In the STD case, isoprene has a pronounced diurnal cycle with a peak in the early afternoon and a minimum just before sunrise (Figure 1a). This diurnal pattern of isoprene has been observed in many forests ranging from deciduous to tropical under clear and well-mixed conditions (Apel, 2002; Wei et al., 2018) and is well captured by models of different scales (Ashworth et al., 2015; de Arellano et al., 2011). During the 2016 AMOS field campaign at UMBS, an EOD peak in isoprene was observed during clear and calm days. The peak occurs around 21:00 local time (LT) when the emissions are near 0 (sunset is around 21:30 LT). Isoprene increases by over 3 ppbv from 19:00 LT to 21:00 LT followed by a precipitous decline in the next 2 hr (Figure 1a).

During the daytime, air temperature in the EOD case is on average 8°C lower than that in the STD case (Figure 1d), indicating less surface heating and thus weaker mixing in the EOD case, demonstrated by the decrease in the midday standard deviation of vertical velocity (σ_w) by a factor of 2 (Figure 1c). During the day-to-night transition period, both case studies show clear (cloudless) conditions (Figure 1b) that favor the radiative cooling of the canopy and thus the development of a more stable boundary layer. In a stable boundary layer, thermal stratification leads to the destruction of turbulence and therefore turbulence production depends on wind shear (Van de Wiel, Moene, Jonker, Baas, et al., 2012). Van de Wiel, Moene, Jonker, Baas, et al. (2012) predict that the minimum wind at the crossing level (where the wind is relatively stationary compared to lower and higher levels, typically some decameters above the surface) for sustainable turbulence at the surface is 5–7 m s^{-1} during the day-to-night transition period. The STD case shows wind speed of 5 m s^{-1} at 46 m that appears to be adequate to sustain turbulent mixing as demonstrated by the relatively high σ_w value of 0.7 m s^{-1} throughout the evening (Figures 1c and 1f). In this case, the sustained mixing dominates over the decreasing emission at dusk, leading to decreases in isoprene mixing ratios during the day-to-night transition period.

In the EOD case, however, wind speed is low (around 2 m s^{-1}) and drops to almost 0 at 21:00 LT when the EOD peak occurs (Figure 1f), indicating little mechanical production of turbulence at the time. Consequently, the σ_w decreases to less than 0.1 m s^{-1} around 21:00 LT (Figure 1c). Therefore, we hypothesize that during clear and calm nights, stratification and weak wind suppress turbulent exchanges between the canopy and the air above (also referred to as decoupling), leading to the accumulation of isoprene emitted at dusk in the canopy. In addition to the increase in wind speed, a shift in wind direction from north to south occurs at the same time as the peak, likely influencing the rapid decline of isoprene (Figure 1f; see section 3.3.1).

3.1.2. Relationship Between Isoprene Mixing Ratio and σ_w

To demonstrate the generality of this phenomenon, 7 out of 30 days are identified as EOD (STD) case. The isoprene mixing ratio and σ_w are averaged over all events to show their diurnal evolution (Figure 2). For the EOD case, in-canopy isoprene begins to increase 2 hr before the peak that appears at 21:00 LT (Figure 2a). Due to the time sequencing of the gradient measurements, the actual peak time could be somewhere between 20:35 and 21:00 LT (see section 2.2). Within the 2 hr, the average in-canopy isoprene

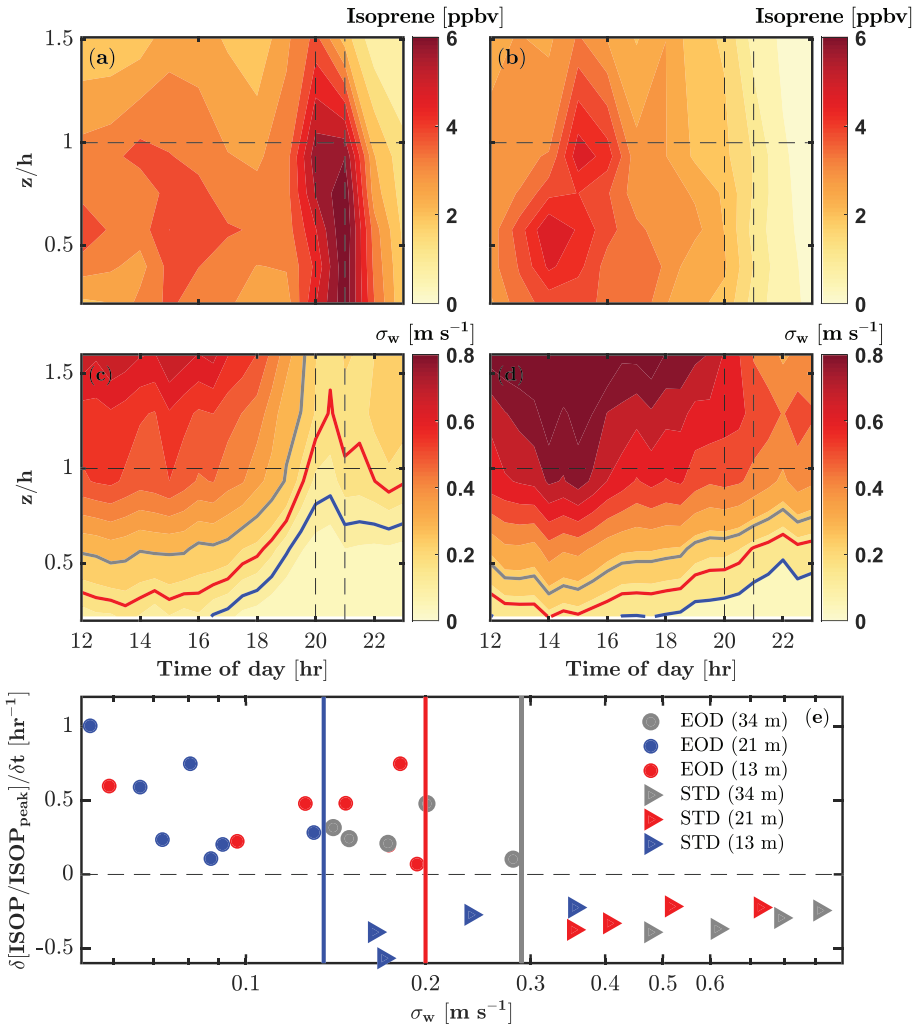

Figure 2. In-canopy profiles of isoprene and σ_w averaged over all EOD (a, c) and STD (b, d) cases. Isoprene mixing ratios as a function of local time and height for the EOD case (a) and STD case (b). Averaged σ_w as a function of local time and height for the EOD case (c) and STD case (d). The vertical dashed lines in Panels (a)–(d) denote the period within 1 hr before the peak (20:00–21:00 local time). The correlation between the changes in isoprene relative to the peak isoprene concentration with time ($\partial \left[\frac{\text{ISOP}}{\text{ISOP}_{\text{peak}}}\right] / \partial t$) and σ_w at heights above the canopy (34 m: gray markers) and in the canopy (21 m: red markers; 13 m: blue markers) (e). Data shown in (e) are prior-peak data only. Critical σ_w values are noted with vertical lines for the three heights for the EOD cases (circles) and the STD cases (triangles). The contour lines for the critical σ_w values are shown in (c) and (d).

increases 77% (from 3.5 to 6.2 ppbv) and the in-canopy σ_w decreases below 0.2 m s^{-1}, indicating that the mixing rate becomes inadequate to transport the isoprene emitted out of the canopy. Within 1 hr of the peak, the above-canopy isoprene ($1.5z/h$) starts to decrease while the in-canopy isoprene ($0.9z/h$) keeps increasing in response to the fact that less and less isoprene is transported out of the canopy, resulting in a significant gradient between the two layers (4 ppbv) at the time of the in-canopy EOD peak (21:00 LT; Figure 2a). This gradient, along with the low σ_w, suggests the decoupling of the canopy layer from the air above and thus the accumulation of isoprene in the canopy. Note that because of the 25 min lag time in the measurement of $1.5z/h$ and $0.9z/h$ (see section 2.2), as well as the opposite trends in isoprene concentrations of the two layers, the 4 ppbv represents the upper bound of the actual gradient. In the STD case, however, no substantial gradients (<1 ppbv) between the above- and in-canopy isoprene is observed at the time of the EOD peak (21:00 LT), and σ_w above the canopy and in the upper canopy is generally greater than 0.4 m s^{-1}, indicating stronger vertical mixing than the EOD case.

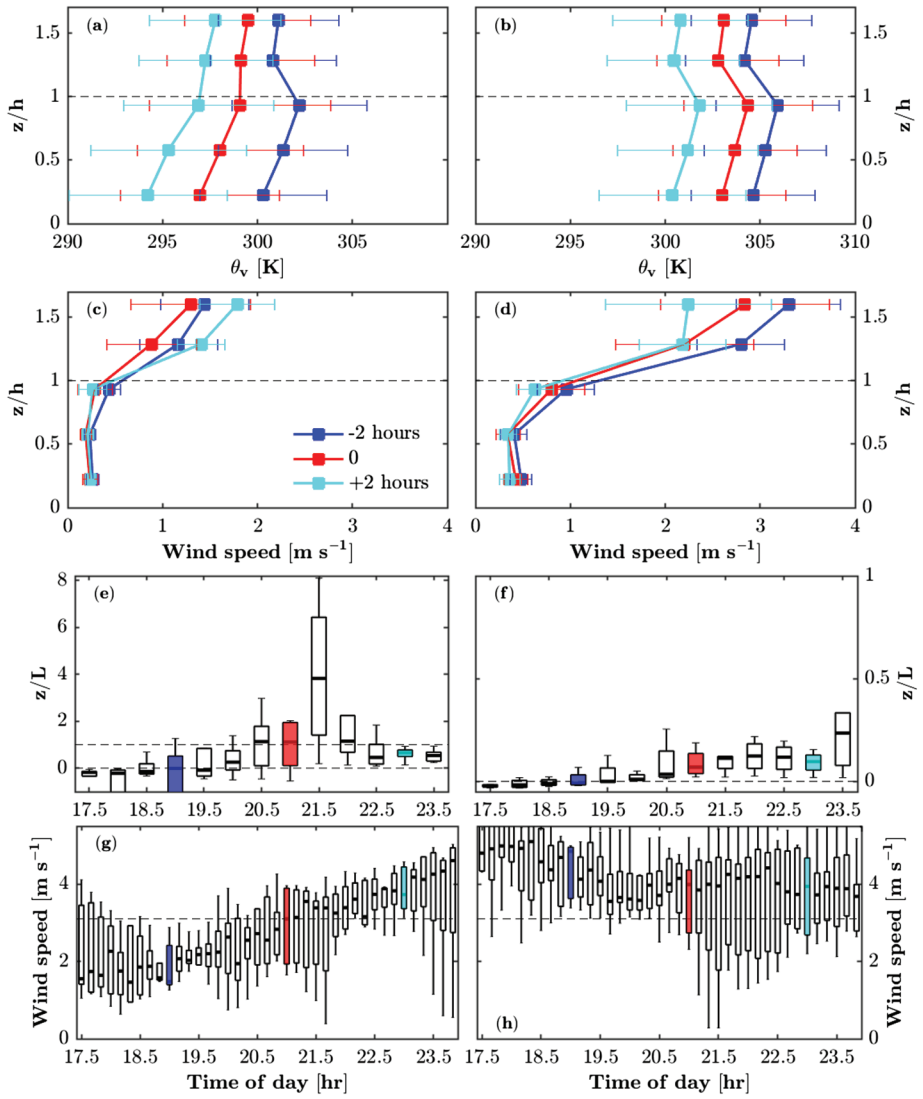

Figure 3. Averaged profiles of virtual potential temperature (θ_v) for the EOD case (a) and STD case (b) for these periods: 2 hr before the peak (blue), the average peak time 21:00 LT (red), and 2 hr after the peak (cyan). Averaged profiles of wind speed from sonic anemometers for the EOD case (c) and STD case (d). The evolution of dimensionless stability parameter z/L for the EOD case (e) and STD case (f) (note different y axis scales for (e) and (f); a dashed line on (e) compares the maximum for (f)). The evolution of wind speed at 46 m for the EOD case (g) and STD case (h).

Isoprene is well mixed throughout the entire canopy during the day-to-night transition period for both EOD and STD cases (Figures 2a and 2b). The large differences in σ_w between the two cases (Figures 2c and 2d) suggest the well-mixed conditions are driven by different processes. For the STD case, no significant decrease in σ_w was observed even after the sunset, indicating that turbulence is continuous through the day-to-night transition, leading to a well-mixed canopy. This result also supports the assertion that turbulent mixing accounts for the isoprene removal during the transition period in the STD case. The continuous turbulence in the STD case is likely sustained by the large-scale forcing (i.e., the relatively high wind speed above the canopy; Figure 3d and 3h). Unlike the STD case, weak turbulence in the EOD case ($\sigma_w < 0.2\,\mathrm{m\,s^{-1}}$) under decoupled conditions is likely generated by local shear instability associated with nonstationary disturbances, such as density currents, drainage flow, and canopy waves (Acevedo & Fitzjarrald, 2003; Alekseychik et al., 2013; Cava et al., 2004). Isoprene emissions at all heights combined with the weak vertical mixing during the decoupling period may contribute to minimal in-canopy gradients in the EOD case.

We use the correlation between the changes in isoprene relative to the peak isoprene concentration with time ($\partial \left[\frac{\mathrm{ISOP}}{\mathrm{ISOP_{peak}}}\right] / \partial t$) and the standard deviation of the vertical velocity (σ_w) to define a critical threshold for

σ_w that could inhibit vertical mixing. This threshold indicates when the emissions dominate over mixing in the late afternoon, and the isoprene mixing ratio starts to increase. The time period (∂t) used here is the 2 hr before the EOD peak for both cases, where isoprene increases in the EOD case and decreases in the STD case. The peak isoprene concentration ($ISOP_{peak}$) is the EOD peak concentration for the EOD case and the highest isoprene concentration for the STD case (i.e., the concentration at the begining of this 2 hr period). A critical σ_w of 0.14, 0.2, and 0.29 m s^{-1} is identified for heights of $0.6z/h$ (13 m), $0.9z/h$ (21 m), and $1.5z/h$ (34 m), respectively (Figure 2e). In the EOD case, σ_w drop below the critical values and isoprene peaks occur, while in the STD case σ_w remain above the critical values in the upper canopy (Figures 2c and 2d). In the EOD case, the rate of increase of isoprene shows little correlation with the magnitude of σ_w, indicating a negligible contribution of mixing on isoprene mixing ratios. For the STD case, the rate of change of isoprene is relatively small and becomes less negative with σ_w above and within the canopy, indicating the varying source strength and/or other sinks (such as chemical losses) associated with different weather conditions. The results here suggest that a critical σ_w can be identified to detect the EOD peak in gases with similar or longer chemical lifetimes as isoprene, and the magnitudes of the critical σ_w depend on the source strength of the gases such as the daily emission cycle.

3.2. Static Stability and Wind Shear

In section 3.1.2, we show a strong relation between low mixing and EOD peak, and in section 3.1.1 we hypothesize that clear and calm nights could drive low mixing. Here, we examine the evolution of the stratification and wind shear during the day-to-night transition period (Figure 3) to provide a mechanistic explanation for the low mixing responsible for the EOD peak and subsequent isoprene removal.

Overall, the virtual potential temperature (θ_v) in the STD case is higher than that in the EOD case. In the STD case, the θ_v at the floor of the canopy is 1 kelvin (K) lower than the canopy top throughout the day-to-night transition period (Figure 3b), suggesting a weakly stable canopy layer. A weakly stable boundary layer is defined as the regime in which turbulence is continuous and thus the dominant transport process, distinguishable from a very stable boundary layer where turbulence is relatively weak compared to other (sub)mesoscale motions such as waves (Mahrt, 1999; Nieuwstadt, 1984; Steeneveld, 2012). The θ_v at the canopy top is 3 K higher than aloft, suggesting a weakly unstable layer above the canopy (Figure 3b). This is likely caused by the heat storage of the canopy based on the large temperature difference between the STD and the EOD cases. Overall, the averaged temperature gradients are small (<3 K). The day-to-day variations in θ_v (as shown by the error bars in Figures 3a and 3b) are generally larger than the vertical gradients. However, we note that only two levels of pressure data (36 and 6 m) are available for the calculation of the θ_v (see section 2.3.1) and as a result, we may be underestimating the θ_v gradient. To complement the θ_v data set, we also examine the dimensionless stability parameter (z/L) that expresses the relative roles of shear and buoyancy in the production of turbulence. Values greater than 0 indicate stable conditions, while values less than 0 indicate unstable conditions. Mahrt (1998) divide the stable boundary layer into three stability regimes as a function of z/L: (i) weakly stable regime ($0 < z/L < O(0.1)$); (ii) intermediate regime ($O(0.1) < z/L < O(1)$) where the strength of turbulence decreases rapidly with increasing stability; (iii) very stable regime ($z/L > O(1)$). In the STD case, the boundary layer becomes stable after 19:00 LT as z/L became positive (Figure 3f). The z/L is generally less than 0.1, indicating a weakly stable boundary layer. This is in agreement with the results from the θ_v profiles described above. In a weakly stable boundary layer, continuous turbulence in the evening can only be sustained by wind shear. The wind speed above the canopy (>2 m s^{-1} at 36 m and >4 m s^{-1} at 46 m) is relatively high (Figures 3d and 3h) and appears to sustain the continuous turbulence as shown in Figure 2d, suggesting the wind speed here is above the minimum wind speed for sustainable turbulence proposed by (Van de Wiel, Moene, Jonker, Baas, et al., 2012). In summary, the high wind speed (>4 m s^{-1} at 46 m) is able to sustain the turbulence in the stable boundary layer during the day-to-night transition period.

For the EOD case, a stable boundary layer evolves early in the evening and becomes less stable later at night (Figures 3a and 3e). Two hours before the EOD peak, even though the canopy layer is already stable, the θ_v at the canopy top is 2 K higher than in the overlying air, suggesting a weakly unstable air layer between $z/h = 1$ and $z/h = 1.5$. As the radiative cooling continues, a very stable layer is established over the EOD period (19:30–21:30 LT), demonstrated by the z/L values reaching 4. This large z/L is likely forced by the near-zero winds (Figure 3g) that cause a very small L. Turbulence production then depends on wind shear

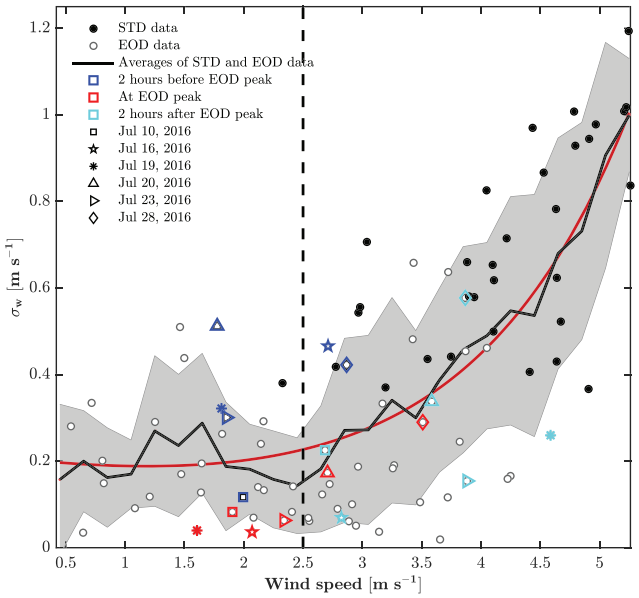

Figure 4. Dependence of σ_w on wind speed. Markers denote observations for the STD case (solid black circles) and the EOD case (open black circles). The data points of 2 hr before (blue), at (red), and 2 hr after the EOD peaks (cyan) are color coded with different symbols denoting different EOD peak days (the turbulence data for 4 July 2016 are missing). The bin-averaged (bin width is 0.25 m s^{-2}) data (black line and the shaded area) and the fitting curve (red line) are also shown. The σ_w data measured at 34 m and wind speed data at 46 m are used in this figure.

in the stable boundary layer. Wind speed above the canopy is low (<1.5 m s^{-1}; Figure 3c), suggesting little wind shear production. Even though the wind speed above the canopy (46 m) continues to increase during this period (Figure 3g), the turbulence is still weak as shown in section 3.1.2. These results indicate, unlike the STD case, the wind speed above the canopy (<3.4 m s^{-1} at 46 m and <1.5 m s^{-1} at 36 m) is inadequate to sustain the turbulence. Therefore, the combination of stratification and weak wind lead to the reduction of turbulence during the EOD period (19:30–21:30 LT).

As the wind increases progressively after the EOD peak (Figure 3g), the z/L values drop to less than 1 (Figure 3e), indicating the transition from a very stable canopy layer to a less stable canopy layer. Previous studies (Mahrt et al., 2012; Russell et al., 2016; Sun et al., 2012) show that there is a threshold point at which stable condition turbulence switches from being independent of wind speed to being dependent on wind speed. During the EOD period (19:30–21:30 LT), the turbulence does not respond to the increase in wind speed. However, after the wind speed becomes greater than a certain value (>3.4 m s^{-1} at 46 m; Figure 3g), the stability is reduced (Figure 3e) and σ_w above the canopy increases (Figure 2c).

The dependence of σ_w on the mean wind speed is explored to identify the threshold wind speed and thus to illustrate the recovery of turbulence in the EOD case (Figure 4). A clear relation between the σ_w and the wind speed exits when the wind speed (u) is greater than 2.4 m s^{-1} (Figure 4). Sun et al. (2012) define a threshold wind speed, after which turbulence intensity increases rapidly using the correlation of the turbulence intensity with the mean wind speed. According to Sun et al. (2012), the value of 2.4 m s^{-1} can be identified as the threshold wind speed using Figure 4. In addition, the data suggest a two-term exponential form ($\sigma_w = 0.18e^{-0.17u} + 0.02e^{0.75u}$, $R^2 = 0.98$) with the second term accounting for the rapid increase of σ_w at higher wind speeds and both terms explaining the slow increase of σ_w at lower wind speeds. We define the wind speed where the second term becomes dominant over the sum of the two terms (i.e., $\frac{\text{term2}}{\text{term1+term2}} > 50\%$) as the threshold value. This gives a threshold wind speed of 2.5 m s^{-1} that is in agreement with the value (2.4 m s^{-1}) identified using Figure 4 as well as previous studies on the stable boundary layer in forested environments (e.g., Russell et al., 2016).

Turbulence in the stable boundary layer has been categorized into various regimes based on different governing variables or threshold values (de Wiel et al., 2003; Mahrt, 1999; Sun et al., 2012). For example, Sun et al. (2012) uses the threshold wind speed to define turbulent regimes, including (i) Regime 1 (u< 2.5 m s^{-1}), a weak turbulence regime where the σ_w shows little dependence on the mean wind speed u; (ii) Regime 2 (u> 2.5 m s^{-1}), a strong turbulence regime when the σ_w increases rapidly with u. The σ_w in Regime 1 is predominately from 2 hr before and at the EOD peaks. These σ_w at the EOD peak (red symbols in Figure 4) increase as the wind speed exceeding the threshold value after the EOD peaks (cyan symbols in Figure 4), suggesting the reenhancement of turbulence. The σ_w of Regime 2 are predominantly from the STD case and the postpeak with two exceptions (20 and 28 July 2016). However, the increases in the σ_w after the EOD peaks in these two cases still suggest the reinstate of the turbulence by the winds as other EOD cases. Some of the postpeak σ_w are still below the critical σ_w (0.29 m s^{-1}, Figure 2e), however, the critical σ_w is based on changes in isoprene before the peak occurs when emissions are still occurring. In the postpeak period (21:00–22:00 LT), emissions have likely ceased and lower σ_w is required to reduce isoprene concentrations. In summary, the wind speed of 2.5 m s^{-1} can be considered as the threshold wind speed where turbulence becomes dependent on the mean wind speed in this study. For the EOD case, turbulence is reduced due to stratification and weak wind during the clear and calm nights, leading to the EOD peak (i.e., accumulation of isoprene in the canopy). However, the wind speed above the canopy increases to the threshold value after the EOD peak, and turbulence is then reinstated. The recovery of turbulence produced by wind shear plays an importance role in the rapid isoprene removal (see section 3.3.1).

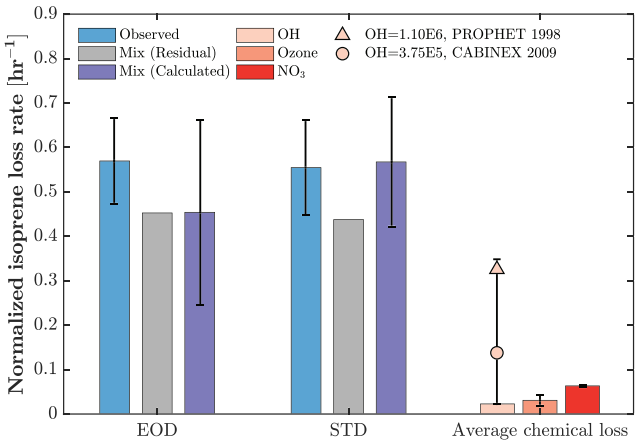

Figure 5. The loss rates of isoprene from 21:00 LT to 22:00 LT. Isoprene loss rate calculated from the observed isoprene mixing ratios (blue). Chemical loss with respect to hydroxyl radicals OH (pink), ozone (orange), and nitrate radicals NO_3 (red). Estimated isoprene loss rate due to vertical mixing (gray) as the differences between the observed (blue) and the chemical losses (pink, orange, and red). Estimated isoprene loss rate due to vertical mixing using the sonic anemometer data (Equation 4; purple). Isoprene chemical loss rates with respect to OH from previous campaigns at the same site (Faloona et al., 2001; Griffith et al., 2013) (triangle and circle). Error bars represent day-to-day variations. The error bar for OH also includes measurement uncertainty.

3.3. Nighttime Removal of Isoprene

3.3.1. Contributions of Chemistry and Vertical Mixing to the Nighttime Removal

The observed isoprene loss rates from 21:00 LT to 22:00 LT are 0.57 and 0.55 hr^{-1} on average for the EOD and STD case, respectively (Figure 5). The similar magnitude of the two loss rates suggests that the processes responsible for this rapid decline are similar. Previous studies also report similar loss rates of isoprene at this study site (Hurst et al., 2001) as well as in other forested sites (Doughty et al., 2013). Assuming horizontal homogeneity at the study site, the possible nighttime sinks for isoprene are vertical mixing and chemical reactions with OH, ozone (O_3), and nitrate radicals (NO_3). No significant dry deposition of isoprene has been observed to date, probably due to its nonpolar structure (Hurst et al., 2001) and the high surface resistance (Wesely, 2000). In this section, we constrain the possible loss rates noted above using available observations.

Because the in-canopy rapid decay typically initiates between 21:00 p.m. and 22:00 p.m. (refered to as "the decay period" hereinafter), the average concentrations of the oxidants (OH, O_3, and NO_3) over this period are used to calculate the chemical loss rates. The AMOS 2016 campaign-average OH is 6.19×10^4 cm^{-3} for the decay period, resulting in an average loss rate of 0.02 hr^{-1} (Figure 5). The standard deviation (1σ) of the measured OH is 8.86×10^5 cm^{-3} and represents the daily variations as well as the precision of the measurements from the top of the tower. The uncertainty associated with the calibration of the OH instrument is approximately 18% (Dusanter et al., 2008). The PROPHET 1998 (Program for Research on Oxidants: PHotochemistry, Emissions, and Transport) and the CABINEX 2009 (Community Atmosphere-Biosphere INteractions EXperiment) campaigns at this study site reported an average nighttime OH concentrations of 1.1×10^6 cm^{-3} measured by the Penn State laser-induced fluorescence (LIF) instrument (Faloona et al., 2001) and 3.75×10^5 cm^{-3} measured by the Indiana University Fluorescence Assay by Gas Expansion (IU-FAGE) instrument (Griffith et al., 2013), respectively. These concentrations are approximately 18 and 6 times higher than that measured during AMOS 2016. Recent studies have noted that unknown interferences may contribute to the reported OH concentrations in LIF measurements that only used a wavelength modulation technique without a chemical removal system (Feiner et al., 2016). This is one possible explanation for the higher nighttime OH concentrations obtained during the PROPHET 1998 and CABINEX 2009 campaigns. Measurements of potential interferences associated with the IU-FAGE instrument during CABINEX 2009 suggest that an unknown interference potentially accounts for 50–100% of the nighttime OH concentrations (Griffith et al., 2013). However, as discussed above, the chemical removal system used during AMOS 2016 did not reveal any significant interference, suggesting that the measured concentration during the in-canopy decay period accurately reflect the ambient OH concentration above the canopy. Given the low radiation and high isoprene concentrations in the canopy in the early evening, the OH concentration in the canopy may be even lower than that above the canopy. Therefore, the observed OH concentrations are inadequate

to account for the observed isoprene loss rates at night at the study site, yet more precise and accurate measurements are needed to reduce the uncertainties.

Reaction of O_3 with isoprene is much slower than with OH. The average O_3 mixing ratios during the decay period are 28(±11) ppbv and 20(±9) ppbv for the STD and EOD case, respectively. O_3 measurements were made in the trunk space (6 m) where O_3 concentrations are generally lower than those in upper canopy and above canopy especially when vertical mixing is low (Freire et al., 2017). Therefore, the lower O_3 concentrations in the EOD case provide additional support to the likelihood of low vertical mixing driving the EOD isoprene peak. Given that the mixing remains relatively high in the STD case, O_3 is assumed to be well mixed and represent the concentrations in the upper canopy. Therefore, the O_3 concentrations in the STD case (28 ± 11 ppbv) were used to calculate the isoprene loss rate, leading to 5(±2)% of the observed isoprene loss rate for both cases. Note that this loss rate acts as an upper bound for the EOD case, as the lower mixing would also reduce O_3 transport into the canopy.

NO_3 has been shown to be the main factor for nighttime isoprene decay in high-NO_X regions (Brown et al., 2009; Doughty et al., 2013; Millet et al., 2016). An average NO_X level of 0.77(±0.73) ppbv and 0.70(±0.62) ppbv were observed during the decay period for the EOD and STD case respectively, indicating clean conditions at the study site. The combination of low NO_X and aforementioned low O_3 levels results in NO_3 mixing ratios that are always below the limit of detection of the instrument (LOD = 1.4 pptv) during the decay period for both cases. In fact, 93% of the NO_3 measured during the entire campaign are below LOD with a maximum of 3.9 pptv. Measurements at other clean forest sites also show that NO_3 mixing ratios in the canopy are nearly always below a LOD of 1.3−1.4 pptv (Liebmann et al., 2018). If all isoprene loss were attributed to reaction with NO_3, the observed isoprene loss rates would require a NO_3 of 10 pptv on average, which would be an order of magnitude larger than observed. Therefore, NO_3 is not expected to be large enough to cause the observed isoprene removal at the study site. Because all measurements are below the LOD, we use the Forest Canopy Atmosphere Transfer model (Ashworth et al., 2015), as constrained by isoprene, O_3, NO_X measurements, to estimate NO_3. An estimate of 1.1(±0.05) pptv was obtained, accounting for only 11(±0.5)% of the observed isoprene loss rates for both cases (Figure 5). Hurst et al. (2001) estimate an maximum NO_3 of 1.7 pptv for an NO_2 and O_3 of 1.0 and 77.1 ppbv during the decay period for the same study site. Our estimate of NO_3 is slightly lower due to the lower NO_2 and O_3 concentrations observed.

In summary, the chemical losses in total can account for 20% of the observed isoprene loss rates for both EOD and STD cases. The largest uncertainty in the chemical loss estimation described above lies in the dusk-to-nighttime OH concentrations. For example, if the true OH conctrations during the decay period were higher than the reported values by an average of 1σ, OH removal could explain up to 60% of the observed isoprene loss (Figure 5).

To estimate the isoprene loss rate due to turbulent mixing, we use a residual method. The residual (LR_mix_res) between the observed and the total chemical losses are then considered as the contribution by mixing, accounting for 80% of the observed loss rates for both EOD and STD case on average. The estimated loss rate in response to vertical mixing (LR_mix_est) is calculated from the sonic anemometer data using Equation 4. This estimate is similar to the residual for the EOD case (LR_mix_est = $0.45 \pm 0.21\ hr^{-1}$; LR_mix_res = $0.45\ hr^{-1}$) and 30% higher than the residual for the STD case (LR_mix_est = $0.57 \pm 0.15\ hr^{-1}$; LR_mix_res = $0.44\ hr^{-1}$). Discrepancies between the two estimates (LR_ mix_ res and LR_ mix_ est) may be attributed to (i) uncertainties in the estimation of LR_ mix_ est associated with the choice of stable boundary height and the value of $[ISOP]_{above}/[ISOP]_{in\text{-}canopy}$ (section 2.3); and/or (ii) the lack of interactions between physical and chemical processes in LR_ mix_ res which could be important under stable/nighttime conditions (Freire et al., 2017). For example, incomplete mixing could cause segregation between isoprene and OH and thus reduction in the reaction rates (Kim et al., 2016), which would lead to a lower chemical loss rate and then a higher residual loss rate due to mixing. Overall, the LR_ mix_ est agree with LR_mix_res. Note that the similarity of the loss rates between the EOD and STD cases (Figure 5) suggests that the main process responsible for this rapid decline are similar (i.e., turbulent mixing). This is supported by the sustained turbulence by the continuously high wind speeds in the STD case, and by the reintroduction of turbulent mixing by increased winds above the canopy in the EOD case.

Further evidence of turbulent mixing accounting for the observed isoprene loss rates could be supported by positive isoprene fluxes above the canopy during the decay period. However, the isoprene flux data are not valid because of low turbulence (the friction velocity $u_* < 0.2\ m\ s^{-1}$) during the decay period for the EOD

case. For the STD case, the average isoprene flux (F_{OBS}) during the decay period is 0.01(±0.01) ppbv m s^{-1}. To establish a metric to explain and assess the magnitude of the observed flux, a flux gradient method (i.e., $F_{Cal} = -K\frac{\Delta C}{\Delta z}$) was used to estimate the isoprene fluxes. The calculation suggests an average of 0.18 and 0.03 ppbv m s^{-1} for F_{Cal} for the EOD and STD case, respectively. The estimated and measured isoprene fluxes are in the same order of magnitude for the STD case, serving as a verification of the fidelity of the flux gradient method for the decay period. From flux gradient theory, it is reasonable to suppose a higher isoprene flux in the EOD case given the greater concentration gradient ($\Delta C_{EOD} = -3.84$ ppbv, $\Delta C_{STD} = -0.42$ ppbv) but similar eddy diffusivity ($K_{EOD} = 0.62$ m^2 s^{-1}, $K_{STD} = 0.89$ m^2 s^{-1}). However, the observations did not capture the fluxes corresponding to the removal of the accumulated isoprene for the EOD case. There are several possible reasons for this discrepancy. First, the majority of the isoprene fluxes associated with the EOD peak might not be captured by the flux measurements measured 30 min later due to the time differences between the gradient and flux observations (see section 2.3). Second, eddies associated with the weak turbulence transporting isoprene out of the canopy during the decay period in the EOD case might be too small to be captured by the eddy covariance system placed at 10 m above the canopy. The calculation-observation discrepancy also raises a possibility that the assumption of horizontal homogeneity used here is invalid for the EOD case at the study site (see discussion in section 3.3.2).

3.3.2. Influences of Advection on the Nighttime Removal

Section 3.2 described the observed increased wind speed to a critical value and its effect of increasing the turbulent mixing in the EOD case, indicating that synoptic forcing becomes important in the stable boundary layer. In this study, a wind direction shift from the north to the south was observed along with the increase in wind speed for 85% of the EOD peak events (e.g., Figure 1f). Because this wind direction shift occurs after the isoprene peak, we hypothesize that horizontal advection is an important driver of the nighttime isoprene decline. This shift in wind direction resembles lake breeze that has been observed in the Great Lake regions (Moroz, 1967). The lake breeze is most frequently observed in July and August due to the minimal daytime cloudiness and the low wind speeds that maximize the land-lake temperature differences in the Great Lake regions (Ryznar & Touma, 1981). Note that the clear and calm conditions during which the EOD peak developed also favor the lake breezes by enhancing the land-lake temperature differences.

The lake breeze phenomenon would introduce another uncertainty (i.e., advection) in the investigation of nighttime isoprene removal. Assuming horizontal homogeneity (i.e., no advection) for simplicity and analytical tractability, we show the rapid removal of isoprene could be driven by vertical mixing for the EOD case (section 3.3.1). However, Sun et al. (1998) showed that a lake breeze could generate a significant advection for CO_2. If this is the case for isoprene, the small fluxes measured above the canopy as well as the rapid isoprene removal could be due to the significant advection dominating over the vertical mixing. This hypothesis of advection is supported by the increased wind and the wind direction shift (Figures 1e, 1f, 3c, and 3g). The advection can be estimated by vertical flux divergence measurements made on very tall towers (Lee & Hu, 2002), yet these measurements do not exist at the site. More data are required to validate the occurrence of lake breeze and quantify the contribution of advection in the nighttime isoprene removal.

4. Summary and Conclusions

Seven days (23% of the measurement period) during the 2016 AMOS field campaign are identified as having an EOD peak in isoprene mixing ratio. The peak occurs around sunset (21:30 local time) and the in-canopy isoprene increases by 77% (from 3.5 to 6.2 ppbv) on average. Stratification and weak wind (<3.4 m s^{-1} at 46 m) during clear and calm nights significantly suppress turbulent exchanges between in- and above-canopy, leading to the accumulation of isoprene emitted at dusk in the canopy, observed as the EOD peak. A critical σ_w of 0.14, 0.2, and 0.29 m s^{-1} is identified to detect the EOD peak for the height of 13, 21, and 34 m, respectively. As wind speeds increases, mixing recovers to reduce isoprene mixing ratios. Observed shifts in wind direction suggests that the increased wind speed could be attributed to the lake breezes. When the wind speed increased above 2.5 m s^{-1}, turbulence is enhanced again. Therefore, a wind speed of 2.5 m s^{-1} is considered as the threshold point where turbulence switches from being independent of wind speed to dependent on wind speed. However, in the standard case where wind speed is greater than the threshold point throughout the evening hours, turbulence is sustained (σ_w> 0.4 m s^{-1}) by wind shear and no EOD peak is observed.

The observed isoprene exhibit similar loss rates for the EOD and standard cases of 0.57 and 0.55 hr^{-1} on average, respectively. Measured OH, O_3, and NO_3 suggest that chemical losses in total accounts for 20% of

the observed loss rate for both cases. The largest uncertainty in the chemical loss estimation is associated with the OH instrument. Estimated turbulent mixing timescales suggest that turbulent mixing accounts for the remaining 80% of the observed loss rates. Observations did not capture the fluxes corresponding to the turbulent removal of the accumulated isoprene in the canopy, and this may be due to the sampling intervals used to quantify both fluxes and concentration gradients or challenges in micrometeorological methods under stable conditions. Another possible reason is that advection induced by the lake-breeze-like motion dominates over the vertical mixing, indicating the assumption of horizontal homogeneity may not be valid under calm and clear nighttime conditions at the study site. However, measurements do not exist at the site to test this hypothesis.

In summary, stagnant days characterized with clear and calm conditions promote the cooling of the canopy and thus low mixing conditions that lead to the EOD peak. These stagnant conditions are unable to sustain the isoprene peak for more than 2 hr due to enhanced wind speed generated by the developments of a lake-breeze-like motion in the atmosphere. This interesting behavior of isoprene has been reported in many forested regions, but none of previous work provided a clear explanation that accounts for both physical and chemical processes. This study presents representative atmospheric dynamics and chemistry data for temperate forest sites and discuss the possible mechanisms, providing a frame of reference for understanding in-canopy behaviors of reactive gases in forested environments. In addition, these results highlight unique features about reactive in-canopy chemistry. Models are known to have difficulties capturing transitions in the boundary layer from dawn to dusk, and this study illuminates the processes of isoprene in the canopy and its transfer to the free troposphere.

Data Availability Statement

Data are available through Alwe et al. (2019).

Acknowledgments
We acknowledge support by National Oceanic and Atmospheric Administration under grant NA18OAR4310116. D. B. M. and H. D. A. acknowledge support from the National Science Foundation (grants 1932771 and 1428257). M. L., B. B., and P. S. acknowledge grants from the National Science Foundation (AGS-1440834 and AGS-1827450).

References

Acevedo, O. C., & Fitzjarrald, D. R. (2003). In the core of the night-effects of intermittent mixing on a horizontally heterogeneous surface. *Boundary-Layer Meteorology*, *106*(1), 1–33. https://doi.org/10.1023/A:1020824109575

Alekseychik, P., Mammarella, I., Launiainen, S., Rannik, Ü., & Vesala, T. (2013). Evolution of the nocturnal decoupled layer in a pine forest canopy. *Agricultural and Forest Meteorology*, *174–175*, 15–27. https://doi.org/10.1016/j.agrformet.2013.01.011

Alwe, H. D., Millet, D. B., Chen, X., Raff, J. D., Payne, Z. C., & Fledderman, K. (2019). Oxidation of volatile organic compounds as the major source of formic acid in a mixed forest canopy. *Geophysical Research Letters*, *46*, 2940–2948. https://doi.org/10.1029/2018GL081526

Apel, E. C. (2002). Measurement and interpretation of isoprene fluxes and isoprene, methacrolein, and methyl vinyl ketone mixing ratios at the PROPHET site during the 1998 intensive. *Journal of Geophysical Research*, *107*(D3), 4034. https://doi.org/10.1029/2000JD000225

Ashworth, K., Chung, S. H., Griffin, R. J., Chen, J., Forkel, R., Bryan, A. M., & Steiner, A. L. (2015). FORest canopy atmosphere transfer (FORCAsT) 1.0: A 1-D model of biosphere–atmosphere chemical exchange. *Geoscientific Model Development*, *8*(11), 3765–3784. https://doi.org/10.5194/gmd-8-3765-2015

Brown, S. S., deGouw, J. A., Warneke, C., Ryerson, T. B., Dubé, W. P., Atlas, E., et al. (2009). Nocturnal isoprene oxidation over the northeast United States in summer and its impact on reactive nitrogen partitioning and secondary organic aerosol. *Atmospheric Chemistry and Physics*, *9*(9), 3027–3042. https://doi.org/10.5194/acp-9-3027-2009

Burns, S. P., Sun, J., Lenschow, D. H., Oncley, S. P., Stephens, B. B., Yi, C., et al. (2010). Atmospheric stability effects on wind fields and scalar mixing within and just above a subalpine forest in sloping terrain. *Boundary-Layer Meteorology*, *138*(2), 231–262. https://doi.org/10.1007/s10546-010-9560-6

Cava, D., Giostra, U., Siqueira, M., & Katul, G. (2004). Organised motion and radiative perturbations in the nocturnal canopy sublayer above an even-aged pine forest. *Boundary-Layer Meteorology*, *112*(1), 129–157. https://doi.org/10.1023/B:BOUN.0000020160.28184.a0

Claeys, M. (2004). Formation of secondary organic aerosols through photooxidation of isoprene. *Science*, *303*(5661), 1173–1176. https://doi.org/10.1126/science.1092805

Cooper, O. R., Moody, J. L., Thornberry, T. D., Town, M. S., & Carroll, M. A. (2001). PROPHET 1998 meteorological overview and air-mass classification. *Journal of Geophysical Research*, *106*(D20), 24,289–24,299. https://doi.org/10.1029/2000JD900409

de Arellano, J. V.-G., Patton, E. G., Karl, T., van den Dries, K., Barth, M. C., & Orlando, J. J. (2011). The role of boundary layer dynamics on the diurnal evolution of isoprene and the hydroxyl radical over tropical forests. *Journal of Geophysical Research*, *116*, D07304. https://doi.org/10.1029/2010JD014857

de Wiel, B. J. H. V., Moene, A. F., Hartogensis, O. K., Bruin, H. A. R. D., & Holtslag, A. A. M. (2003). Intermittent turbulence in the stable boundary layer over land. Part III: A classification for observations during CASES-99. *Journal of the Atmospheric Sciences*, *60*(20), 2509–2522. https://doi.org/10.1175/1520-0469(2003)060<2509:ITITSB>2.0.CO;2

Doughty, D., Fuentes, J. D., Sakai, R., Hu, X.-M., & Sanchez, K. (2013). Nocturnal isoprene declines in a semi-urban environment. *Journal of Atmospheric Chemistry*, *72*(3–4), 215–234. https://doi.org/10.1007/s10874-012-9247-0

Dusanter, S., Vimal, D., & Stevens, P. S. (2008). Technical note: Measuring tropospheric OH and HO_2 by laser-induced fluorescence at low pressure: A comparison of calibration techniques. *Atmospheric Chemistry and Physics*, *8*(2), 321–340. https://doi.org/10.5194/acp-8-321-2008

Dusanter, S., Vimal, D., Stevens, P. S., Volkamer, R., & Molina, L. T. (2009). Measurements of OH and HO_2 concentrations during the MCMA-2006 field campaign—Part 1: Deployment of the Indiana University laser-induced fluorescence instrument. *Atmospheric Chemistry and Physics*, *9*(5), 1665–1685. https://doi.org/10.5194/acp-9-1665-2009

Faloona, I., Tan, D., Brune, W., Hurst, J., Barket, D., Couch, T. L., et al. (2001). Nighttime observations of anomalously high levels of hydroxyl radicals above a deciduous forest canopy. *Journal of Geophysical Research*, *106*(D20), 24,315–24,333. https://doi.org/10.1029/2000JD900691

Feiner, P. A., Brune, W. H., Miller, D. O., Zhang, L., Cohen, R. C., Romer, P. S., et al. (2016). Testing atmospheric oxidation in an Alabama forest. *Journal of the Atmospheric Sciences*, *73*(12), 4699–4710. https://doi.org/10.1175/JAS-D-16-0044.1

Freire, L. S., Gerken, T., Ruiz-Plancarte, J., Wei, D., Fuentes, J. D., Katul, G. G., et al. (2017). Turbulent mixing and removal of ozone within an Amazon rainforest canopy. *Journal of Geophysical Research: Atmospheres*, *122*, 2791–2811. https://doi.org/10.1002/2016JD026009

Fuchs, H., Hofzumahaus, A., Rohrer, F., Bohn, B., Brauers, T., Dorn, H.-P., et al. (2013). Experimental evidence for efficient hydroxyl radical regeneration in isoprene oxidation. *Nature Geoscience*, *6*(12), 1023–1026. https://doi.org/10.1038/ngeo1964

Goldan, P. D., Kuster, W. C., Fehsenfeld, F. C., & Montzka, S. A. (1995). Hydrocarbon measurements in the southeastern United States: The Rural Oxidants in the Southern Environment (ROSE) program 1990. *Journal of Geophysical Research*, *100*(D12), 25,945–25,963. https://doi.org/10.1029/95JD02607

Griffith, S. M., Hansen, R. F., Dusanter, S., Michoud, V., Gilman, J. B., Kuster, W. C., et al. (2016). Measurements of hydroxyl and hydroperoxy radicals during CalNex-LA: Model comparisons and radical budgets. *Journal of Geophysical Research: Atmospheres*, *121*, 4211–4232. https://doi.org/10.1002/2015JD024358

Griffith, S. M., Hansen, R. F., Dusanter, S., Stevens, P. S., Alaghmand, M., Bertman, S. B., et al. (2013). OH and HO_2 radical chemistry during PROPHET 2008 and CABINEX 2009—Part 1: Measurements and model comparison. *Atmospheric Chemistry and Physics*, *13*(11), 5403–5423. https://doi.org/10.5194/acp-13-5403-2013

Guenther, A. B., Jiang, X., Heald, C. L., Sakulyanontvittaya, T., Duhl, T., Emmons, L. K., & Wang, X. (2012). The model of emissions of gases and aerosols from nature version 2.1 (MEGAN2.1): An extended and updated framework for modeling biogenic emissions. *Geoscientific Model Development*, *5*(6), 1471–1492. https://doi.org/10.5194/gmd-5-1471-2012

Guenther, A. B., Zimmerman, P. R., Harley, P. C., Monson, R. K., & Fall, R. (1993). Isoprene and monoterpene emission rate variability: Model evaluations and sensitivity analyses. *Journal of Geophysical Research*, *98*(D7), 12,609–12,617. https://doi.org/10.1029/93JD00527

Gunsch, M. J., May, N. W., Wen, M., Bottenus, C. L. H., Gardner, D. J., VanReken, T. M., et al. (2018). Ubiquitous influence of wildfire emissions and secondary organic aerosol on summertime atmospheric aerosol in the forested Great Lakes region. *Atmospheric Chemistry and Physics*, *18*(5), 3701–3715. https://doi.org/10.5194/acp-18-3701-2018

Hurst, J. M., Barket, D. J., Herrera-Gomez, O., Couch, T. L., Shepson, P. B., Faloona, I., et al. (2001). Investigation of the nighttime decay of isoprene. *Journal of Geophysical Research*, *106*(D20), 24,335–24,346. https://doi.org/10.1029/2000JD900727

Kim, S.-W., Barth, M. C., & Trainer, M. (2016). Impact of turbulent mixing on isoprene chemistry. *Geophysical Research Letters*, *43*, 7701–7708. https://doi.org/10.1002/2016gl069752

Lee, X., & Hu, X. (2002). Forest-air fluxes of carbon, water and energy over non-flat terrain. *Boundary-Layer Meteorology*, *103*(2), 277–301. https://doi.org/10.1023/A:1014508928693

Lelieveld, J., Butler, T. M., Crowley, J. N., Dillon, T. J., Fischer, H., Ganzeveld, L., et al. (2008). Atmospheric oxidation capacity sustained by a tropical forest. *Nature*, *452*(7188), 737–740. https://doi.org/10.1038/nature06870

Levy, H. (1971). Normal atmosphere: Large radical and formaldehyde concentrations predicted. *Science*, *173*(3992), 141–143. https://doi.org/10.1126/science.173.3992.141

Liang, J., Zhang, L., Wang, Y., Cao, X., Zhang, Q., Wang, H., & Zhang, B. (2014). Turbulence regimes and the validity of similarity theory in the stable boundary layer over complex terrain of the Loess Plateau, China. *Journal of Geophysical Research: Atmospheres*, *119*, 6009–6021. https://doi.org/10.1002/2014JD021510

Liebmann, J., Karu, E., Sobanski, N., Schuladen, J., Ehn, M., Schallhart, S., et al. (2018). Direct measurement of NO_3 radical reactivity in a boreal forest. *Atmospheric Chemistry and Physics*, *18*(5), 3799–3815. https://doi.org/10.5194/acp-18-3799-2018

Liu, C.-M. (2008). Complete solutions to extended Stokes' problems. *Mathematical Problems in Engineering*, *2008*, 1–18. https://doi.org/10.1155/2008/754262

Mahrt, L. (1998). Nocturnal boundary-layer regimes. *Boundary-Layer Meteorology*, *88*(2), 255–278. https://doi.org/10.1023/A:1001171313493

Mahrt, L. (1999). Stratified atmospheric boundary layers. *Boundary-Layer Meteorology*, *90*(3), 375–396. https://doi.org/10.1023/A:1001765727956

Mahrt, L., Richardson, S., Seaman, N., & Stauffer, D. (2012). Turbulence in the nocturnal boundary layer with light and variable winds. *Quarterly Journal of the Royal Meteorological Society*, *138*(667), 1430–1439. https://doi.org/10.1002/qj.1884

Martin, R. S., Westberg, H., Allwine, E., Ashman, L., Farmer, J. C., & Lamb, B. (1991). Measurement of isoprene and its atmospheric oxidation products in a central Pennsylvania deciduous forest. *Journal of Atmospheric Chemistry*, *13*(1), 1–32. https://doi.org/10.1007/BF00048098

Millet, D. B., Alwe, H. D., Chen, X., Deventer, M. J., Griffis, T. J., Holzinger, R., et al. (2018). Bidirectional ecosystem–atmosphere fluxes of volatile organic compounds across the mass spectrum: How many matter? *ACS Earth and Space Chemistry*, *2*(8), 764–777. https://doi.org/10.1021/acsearthspacechem.8b00061

Millet, D. B., Baasandorj, M., Hu, L., Mitroo, D., Turner, J., & Williams, B. J. (2016). Nighttime chemistry and morning isoprene can drive urban ozone downwind of a major deciduous forest. *Environmental Science & Technology*, *50*(8), 4335–4342. https://doi.org/10.1021/acs.est.5b06367

Montzka, S. A., Trainer, M., Goldan, P. D., Kuster, W. C., & Fehsenfeld, F. C. (1993). Isoprene and its oxidation products, methyl vinyl ketone and methacrolein, in the rural troposphere. *Journal of Geophysical Research*, *98*(D1), 1101–1111. https://doi.org/10.1029/92JD02382

Moroz, W. J. (1967). A lake breeze on the eastern shore of Lake Michigan: Observations and model. *Journal of the Atmospheric Sciences*, *24*(4), 337–355. https://doi.org/10.1175/1520-0469(1967)024<0337:ALBOTE>2.0.CO;2

Ng, N. L., Kwan, A. J., Surratt, J. D., Chan, A. W. H., Chhabra, P. S., Sorooshian, A., et al. (2008). Secondary organic aerosol (SOA) formation from reaction of isoprene with nitrate radicals (NO3). *Atmospheric Chemistry and Physics*, *8*(14), 4117–4140. https://doi.org/10.5194/acp-8-4117-2008

Nieuwstadt, F. T. M. (1984). The turbulent structure of the stable, nocturnal boundary layer. *Journal of the Atmospheric Sciences*, *41*(14), 2202–2216. https://doi.org/10.1175/1520-0469(1984)041<2202:TTSOTS>2.0.CO;2

Oliveira, P. E. S., Acevedo, O. C., Moraes, O. L. L., Zimermann, H. R., & Teichrieb, C. (2012). Nocturnal intermittent coupling between the interior of a pine forest and the air above it. *Boundary-Layer Meteorology*, *146*(1), 45–64. https://doi.org/10.1007/s10546-012-9756-z

Rebmann, C., Kolle, O., Heinesch, B., Queck, R., Ibrom, A., & Aubinet, M. (2011). *Data acquisition and flux calculations.* Netherlands: Springer. https://doi.org/10.1007/978-94-007-2351-1_3

Rickly, P., & Stevens, P. S. (2018). Measurements of a potential interference with laser-induced fluorescence measurements of ambient OH from the ozonolysis of biogenic alkenes. *Atmospheric Measurement Techniques*, *11*(1), 1–16. https://doi.org/10.5194/amt-11-1-2018

Robinson, N. H., Hamilton, J. F., Allan, J. D., Langford, B., Oram, D. E., Chen, Q., et al. (2011). Evidence for a significant proportion of secondary organic aerosol from isoprene above a maritime tropical forest. *Atmospheric Chemistry and Physics*, *11*(3), 1039–1050. https://doi.org/10.5194/acp-11-1039-2011

Russell, E. S., Liu, H., Gao, Z., Lamb, B., & Wagenbrenner, N. (2016). Turbulence dependence on winds and stability in a weak-wind canopy sublayer over complex terrain. *Journal of Geophysical Research: Atmospheres*, *121*, 11,502–11,515. https://doi.org/10.1002/2016JD025057

Ryznar, E., & Touma, J. S. (1981). Characteristics of true lake breezes along the eastern shore of lake michigan. *Atmospheric Environment (1967)*, *15*(7), 1201–1205. https://doi.org/10.1016/0004-6981(81)90311-5

Sillman, S., Carroll, M. A., Thornberry, T., Lamb, B. K., Westberg, H., Brune, W. H., et al. (2002). Loss of isoprene and sources of nighttime OH radicals at a rural site in the United States: Results from photochemical models. *Journal of Geophysical Research*, *107*(D5), 4043. https://doi.org/10.1029/2001JD000449

Starn, T. K., Shepson, P. B., Bertman, S. B., Riemer, D. D., Zika, R. G., & Olszyna, K. (1998). Nighttime isoprene chemistry at an urban-impacted forest site. *Journal of Geophysical Research*, *103*(D17), 22,437–22,447. https://doi.org/10.1029/98JD01201

Steeneveld, G. J. (2012). Stable boundary layer issues. In *ECMWF/GABLS Workshop on Diurnal Cycles and the Stable Atmospheric Boundary Layer* (pp. 25–36).

Sun, J., Desjardins, R., Mahrt, L., & MacPherson, I. (1998). Transport of carbon dioxide, water vapor, and ozone by turbulence and local circulations. *Journal of Geophysical Research*, *103*(D20), 25,873–25,885. https://doi.org/10.1029/98JD02439

Sun, J., Mahrt, L., Banta, R. M., & Pichugina, Y. L. (2012). Turbulence regimes and turbulence intermittency in the stable boundary layer during CASES-99. *Journal of the Atmospheric Sciences*, *69*(1), 338–351. https://doi.org/10.1175/JAS-D-11-082.1

Taraborrelli, D., Lawrence, M. G., Crowley, J. N., Dillon, T. J., Gromov, S., Groß, C. B. M., et al. (2012). Hydroxyl radical buffered by isoprene oxidation over tropical forests. *Nature Geoscience*, *5*(3), 190–193. https://doi.org/10.1038/ngeo1405

van Gorsel, E., Harman, I. N., Finnigan, J. J., & Leuning, R. (2011). Decoupling of air flow above and in plant canopies and gravity waves affect micrometeorological estimates of net scalar exchange. *Agricultural and Forest Meteorology*, *151*(7), 927–933. https://doi.org/10.1016/j.agrformet.2011.02.012

Van de Wiel, B. H. L., Moene, A. F., & Jonker, H. (2012). The cessation of continuous turbulence as precursor of the very stable nocturnal boundary layer. *Journal of the Atmospheric Sciences*, *69*(11), 3097–3115. https://doi.org/10.1175/JAS-D-12-064.1

Van de Wiel, B. H. L., Moene, A. F., Jonker, H. J. J., Baas, P., Basu, S., Donda, J. M. M., et al. (2012). The minimum wind speed for sustainable turbulence in the nocturnal boundary layer. *Journal of the Atmospheric Sciences*, *69*(11), 3116–3127. https://doi.org/10.1175/JAS-D-12-0107.1

VanReken, T. M., Mwaniki, G. R., Wallace, H. W., Pressley, S. N., Erickson, M. H., Jobson, B. T., & Lamb, B. K. (2015). Influence of air mass origin on aerosol properties at a remote Michigan forest site. *Atmospheric Environment*, *107*, 35–43. https://doi.org/10.1016/j.atmosenv.2015.02.027

Wei, D., Fuentes, J. D., Gerken, T., Chamecki, M., Trowbridge, A. M., Stoy, P. C., et al. (2018). Environmental and biological controls on seasonal patterns of isoprene above a rain forest in central Amazonia. *Agricultural and Forest Meteorology*, *256–257*, 391–406. https://doi.org/10.1016/j.agrformet.2018.03.024

Wesely, M. (2000). A review of the current status of knowledge on dry deposition. *Atmospheric Environment*, *34*(12–14), 2261–2282. https://doi.org/10.1016/S1352-2310(99)00467-7